Iron silicide wires patterned by Bi nanolines on the H/Si(001) surface: Spin density functional calculations

R. H. Miwa,[1] W. Orellana,[2] and G. P. Srivastava[3]
[1]*Instituto de Física, Universidade Federal de Uberlândia, CP 593, CEP 38400-902, Uberlândia, MG, Brazil*
[2]*Departamento de Ciencias Físicas, Facultad de Ingeniería, Universidad Andres Bello, Av. República 252, 837-0134, Santiago, Chile*
[3]*School of Physics, University of Exeter, Stocker Road, Exeter EX4 4QL, United Kingdom*
(Received 3 October 2007; revised manuscript received 19 May 2008; published 11 September 2008)

The possibility of designing iron silicide wires along Bi nanolines on the hydrogenated Si(001) surface is addressed by spin-density functional calculations. We study plausible adsorption sites for various submonolayer (ML) coverages of Fe atoms along the nanolines. It is found that for a lower coverage of 1/8 ML, Fe atoms are adsorbed beside the Bi nanoline forming sevenfold coordinate structures with the Si subsurface layer. For 1/4 ML coverage, Fe atoms form a linear chain parallel to the nanolines with a semiconducting character, whereas for 1/2 ML coverage they form a zigzag chain with a metallic character. For the increased coverage of 3/4 ML the metallic character is maintained and the Fe atoms are accommodated between the second- and third-Si layers. The calculated formation energy of Fe adatoms decreases with increasing coverage, supporting the formation of iron silicide wire parallel to the Bi nanolines. In addition, for Fe coverages higher than 1/4 ML, the systems exhibit weak antiferromagnetic states which are almost energetically degenerated with their respective nonmagnetic states, suggesting that Fe adatoms have their magnetism quenched as the Fe wire forms. Finally, the orbital and electronic distribution of Fe adatoms on the Bi nanolines is analyzed in term of simulated STM images.

DOI: 10.1103/PhysRevB.78.115310 PACS number(s): 71.15.Nc, 71.20.Nr

I. INTRODUCTION

The electronic and structural properties of nanotubes and nanowires may be tailored in a suitable way through self-assembly processes on solid surfaces. For instance, formation of self-organized arrangements of nanowires[1,2] and nanotubes[3–7] on semiconducting surfaces has been demonstrated. In addition, the surface atomic geometry can be used as a template to grow one-dimensional structures, e.g., indium chains on silicon surfaces.[8–11] It is clear that in such cases the surface topology plays a fundamental role during the atomic organization events.

A unique class of self-organized nanoline formation is achieved by depositing bismuth at about 500 °C on the Si(001) surface.[12–15] The Bi nanolines (NLs) thus formed are approximately 1.5 nm wide and can be several hundred nanometers long and free of defects and kinks. These nanolines do not "illuminate" in scanning tunneling microscope (STM) images taken at low biases,[12] and the resulting surface system is semiconducting. However, the growth of Bi nanolines results in the development of a single domain Si(001) surface,[13] making it possible to use such a system as template to design wire structures with desirable electronic, optical, and even magnetic properties. Indeed, there are some studies addressing the formation of arrays of indium[16,17] and silver[18,19] using the Bi nanolines as a one-dimensional template.

Iron silicide on silicon surfaces has been widely studied, mainly motivated by possible applications in new devices based on silicon technology.[20–24] Using chemical vapor deposition of $Fe(CO)_5$, Adams *et al.*[25] studied the evolution of layer morphology during early stages of Fe adsorption on silicon (001) substrate. Concerning *ab initio* calculations, Kishi *et al.*[26] studied the effect of hydrogen during the initial stages of Fe adsorption on Si(001). Wu *et al.*[24] performed a comprehensive study of thin films of transition-metal silicide on Si(001). Kida *et al.*[27] have also investigated the initial stages of Fe adsorption on Si(001). Their STM studies revealed the formation of self-organized Fe nanowires on water-adsorbed silicon surface $[H_2O/Si(001)]$. It is therefore interesting to examine the possibility of fabricating iron silicide wires by decoration of Bi NLs on the silicon surface.

In this paper we present a detailed first-principles study of the formation of iron silicide wires patterned by the Bi nanolines on hydrogenated Si(001) surface. In particular we examine the equilibrium adsorption sites and the resulting electronic as well as magnetic configuration of a few submonolayer (ML) coverages of Fe adatoms along the Bi nanolines.

II. METHODOLOGY

Our calculations were performed in the framework of the density functional theory,[28] within the local spin-density approximation (LSDA).[29] The electron-ion interaction was treated by using norm-conserving fully-separable pseudopotentials[30] for silicon, hydrogen and bismuth, and ultrasoft pseudopotential for iron.[31] The calculations were performed with the Quantum-ESPRESSO *ab initio* package.[32] The surfaces were simulated by using the slab method, with 10 ML of Si plus a vacuum region of about 10 Å, and surface periodicity of 2×6. A layer of hydrogen atoms was used to saturate the dangling bonds at the bottom silicon layer in the slab. Concerning the Bi NLs structure, in previous works[12,33] we found that the Miki model is energetically more favorable than the Naitoh model (by 0.45 eV/Bi dimer) and that the Haiku model is energetically more favorable than the Miki model (by 0.37 eV/Bi dimer). While the equilibrium atomic geometry of the Miki model is found to be in better agreement with x-ray measurements, STM line

profiles obtained by two groups differ from each other and do not offer conclusive evidence in favor of either the Miki or the Haiku model (see, Ref. 34 and reference therein). In this work, we have, therefore, considered the equilibrium atomic geometry of the Bi NLs as determined within the Haiku model.[35] For the Brillouin-zone sampling we used a set of four special **k** points, and the wave functions were expanded in a plane-wave basis up to a kinetic energy of 25 Ry. The eight topmost layers were fully relaxed within a force convergence criterion of 25 meV/Å.

In order to check the accuracy of our calculations we examine the total energy convergence varying three parameters: (i) the number of special **k** points, (ii) the energy cutoff for the plane-wave basis set, and (iii) the in-plane size of the unit cell. In (i), increasing the number of special **k** points from four to eight we find a decrease in the total energy by 0.08 eV/2×6 unit cell. In (ii), increasing the energy cutoff to 30 Ry we find an energy decrease of 0.01 eV/2×6 unit cell. Finally in (iii), increasing the size of the surface unit cell to 2×7 we find an energy decrease of 0.01 eV/2×7 unit cell. For these tests two structural models with higher concentration of iron adatoms were considered. The above results ensure a good description for the systems under study.

The energetic stability of Fe adatoms forming iron stripes patterned by Bi NLs on the hydrogen passivated silicon surface [hereafter denoted as Bi-NL/H/Si(001)] was determined by the calculation of the formation energy (Ω_i), defined as,

$$\Omega_i = E_i - E_0 - n_{\mathrm{Fe}}\mu_{\mathrm{Fe}}, \tag{1}$$

where E_i represents the total energy of the Fe adatoms patterned by Bi NLs, E_0 represents the total energy of pristine Bi-NL/H/Si(001) system, n_{Fe} indicates the number of Fe adatoms, and μ_{Fe} represents Fe chemical potential calculated from its bulk phase.

III. RESULTS AND DISCUSSION

A. Energetic and structural properties

Initially, we examined the adsorption of Fe atoms on the clean Si(001) surface and compared our findings with the previous *ab initio* total-energy results. We calculated the formation energies for a coverage of one monolayer of Fe adatom in the top (Ω_{top}) and subsurface (Ω_{sub}) interstitial sites as shown in Figs. 1(a) and 1(b) of Ref. 24, respectively. These total-energy calculations were performed by using a 2×1 surface unit cell, and a set of 32 special **k** points for the Brillouin-zone sampling. In this case, E_i in Eq. (1) represents the total energy of Fe adsorbed Si(001) surface, and E_0 represents the total energy of the clean (2×1) reconstructed Si(001) surface. The calculated formation energies, of $\Omega_{\mathrm{sub}}=0.61/(1\times1)$ and $\Omega_{\mathrm{top}}=1.11$ eV/(1×1), indicate an energetic preference of 0.50 eV favoring the Fe adatoms in the subsurface interstitial sites. These results are in accordance with previous *ab initio* calculations performed by Wu *et al.*,[24] using the all-electron full-potential augmented plane wave plus local-orbital method within a generalized gradient approximation. They obtained a total-energy difference of 0.44 eV. At the equilibrium geometry, we find that the subsurface interstitial Fe adatom is sevenfold coordinated, with Fe-Si bond lengths spread between 2.35 and 2.90 Å.

In a previous work we examined the electronic properties and the energetic stability of low coverage Fe adatoms patterned by Bi NLs on H/Si(001).[36] We found that the energetically most stable configuration occurs with Fe adatoms lying beside the Bi NLs, site A1 in Figs. 1(a) and 1(b). In this case there is one Fe adatom within the 2×4 surface area, shown as the shaded region in Fig. 1(a), which corresponds to a Fe coverage of 1/8 ML.

In order to find the formation energy for the Fe adatom on the A1 site, we reproduce the calculation of Ref. 36 using the plane waves basis set used in this work. Our results show that $\Omega_{\mathrm{A1}}=0.92$ eV/unit cell. The Fe adsorption on the hydrogen passivated Si(001) surface (F1) and subsurface (F2) interstitial sites, depicted in Figs. 1(a) and 1(b), are energetically less favorable than A1 by 0.87 and 1.18 eV/unit cell, respectively. This clearly indicates the influence of hydrogen passivation of the substrate on the Fe stabilization along the Bi NLs. Further formation energy calculations (presented below) will show that Fe adatoms lying in A1 work as a seed to the formation of Fe wires patterned by Bi NLs. In addition, we investigate the Fe adsorption on two new sites, at the center of the Bi dimer, configuration D1, and between the two Bi dimers, configuration D2 [see Fig. 1(a)]. We find that D1 and D2 are energetically less stable than A1 by 3.4 and 3.1 eV/unit cell, respectively. In D1, the Bi dimer breaks forming a Bi–Fe–Bi bridge structure, whereas in D2 a similar bridge structure is formed between adjacent Bi dimers, preserving the dimer structures. These clearly show that the Fe-Bi bonds are by far energetically less favorable than the Fe-Si bonds, suggesting that the Bi NLs will preserve their structures after the Fe adsorption.

Figure 1(c) presents the equilibrium geometry of A1 obtained by our present plane-wave calculations. Here, the Fe adatom resides in the subsurface region and is sevenfold coordinated, with Fe-Si bond lengths ranging from 2.2 to 2.7 Å. In addition, the electronic structure calculations showed that for the 1/8 ML coverage the system exhibits a magnetic half-metallic behavior, with majority (spin up) bands showing a semiconducting behavior and the minority (spin down) bands showing metallic behavior. These results are in good agreement with our previous results obtained with localized basis set.[36]

For 1/4 ML coverage we examined different plausible structural models for Fe adatoms on Bi-NL/H/Si(001), by combining the sites show in Figs. 1(a) and 1(b). Our calculated formation energies, listed in Table I, indicate that the structural model A12 (Fe adatoms on A1 and A2 sites), represents the energetically most stable configuration, with $\Omega_{\mathrm{A12}}=0.88$ eV/unit cell. Comparing the formation energies of A1 and A12 we can infer in the existence of an attractive interaction between adsorbed Fe adatoms parallel to the Bi NLs. Therefore, the structural change A1$\rightarrow$A12 is an exothermic process by 0.04 eV/unit cell. On the other hand, by increasing the concentration of Fe adatoms from 1/8 to 1/4 ML, our formation energy results suggest the formation of a wire structure beside the Bi NLs, as depicted in Fig. 1(d).

The other structures with Fe coverage of 1/4 ML are energetically less favorable (see Table I). For instance, during

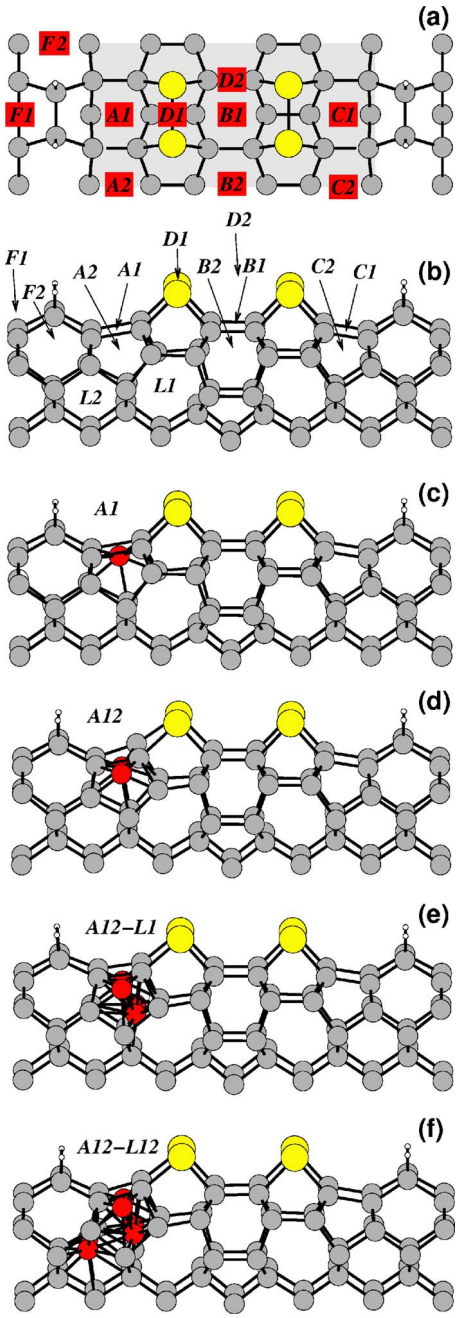

FIG. 1. (Color online) Adsorption sites of Fe adatoms along the Bi nanolines on the hydrogen passivated Si(001) surface. Panels (a) and (b) show the top and side views, respectively, of various plausible adsorption sites with different Fe coverages. Energetically favorable structures as a function of the Fe coverage are shown as: (c) 1/8 ML (A1), (d) 1/4 ML (A12), (e) 1/2 (A12-L1), and (f) 3/4 (A12-L2). Bismuth atoms are represented by yellow circles.

the Fe deposition process instead of Fe adatoms spread out on both sides of the Bi NL, configuration A1C1, there is an energetic preference by 1.14 eV/unit cell that favor the formation of a Fe-wire structure, A12. At this geometry, (i) the Fe adatoms lie 0.5 Å below the topmost Si atoms and are sevenfold coordinated where Fe-Si bond lengths vary from 2.2 and 2.5 Å, (ii) the Si-Bi bond lengths aside the Fe stripe, 2.84 and 2.86 Å, are stretched by ~0.06 Å compared the one on the pristine system (2.79 Å), and (iii) the Bi dimer is slightly buckled vertically by 0.04 Å. Further Fe segregation toward silicon bulk (keeping the Fe coverage of 1/4 ML) has been examined by placing the Fe line in the second subsurface interstitial sites, L1 and L2. We find that the A12 $\rightarrow$L1 and A12$\rightarrow$L2 subsurface segregations are quite unlikely since the total energy increases by 1.14 and 1.62 eV/unit cell, respectively. Thus, we can infer that the formation of a Fe-wire structure (A12) is quite likely beside the Bi NLs for a Fe coverage of 1/4 ML.

TABLE I. Formation energies of Fe structures along the Bi NLs in the equilibrium sites under study (in units of eV/unit cell).

Structure	Fe coverage (ML)	Formation energy (eV)
A1	1/8	0.92
A12	1/4	0.88
B12	1/4	1.42
A1B1	1/4	2.02
L2	1/4	2.02
A1C1	1/4	2.04
A1B2	1/4	2.18
A2C2	1/4	2.42
L1	1/4	2.50
A12-L1	1/2	0.76
A12-C12	1/2	1.00
A12-L2	1/2	1.00
A12-B12	1/2	1.20
A12-L12	3/4	0.42

Concerning magnetic properties, the A12 geometry, show an antiferromagnetic (AFM) state of 0.5 meV/unit cell lower in energy than the nonmagnetic (NM) state. This suggests that for the A12 structure the Fe adatoms exhibit a weak AFM coupling. This is somewhat expected due to the high coordination of Fe adatoms in A12. For this coverage, both majority and minority-spin channels associated to the Fe 3*d* orbitals become fully occupied due to the formation of Fe-Si bonds.

Increasing the Fe coverage up to 1/2 ML, the structural model A12-L1 [Fig. 1(e)] is found to be the most stable. In this structure, the Fe adatoms form a zigzag chain along the fivefold coordinated silicon rings beside the Bi NL. In the equilibrium geometry, the Fe-Fe bond lengths range from 2.5 to 2.7 Å. Further Fe segregation toward the second subsurface site (L2) forms the structural model A12-L2, which is energetically unfavorable by 0.24 eV/unit cell with respect to A12-L1. In addition, A12-L1 also shows an energetic preference with respect to A12-C12 and A12-B12 by 0.24 and 0.44 eV/unit cell, respectively. Since the formation energy of the A12-L1 structure is lower than A12, we can suggest the following scenario when the Fe concentration increases viz.: once a Fe line is formed at the subsurface interstitial sites beside the Bi NL, A12 for Fe coverage of 1/4 ML, further Fe deposition ($1/4 \rightarrow 1/2$ ML) makes likely the formation of a zigzag Fe strip at the subsurface interstitial sites (A12-L1).

Finally, for the Fe coverage of 3/4 ML, we consider the structural model A12-L12 [Fig. 1(f)]. The calculated forma-

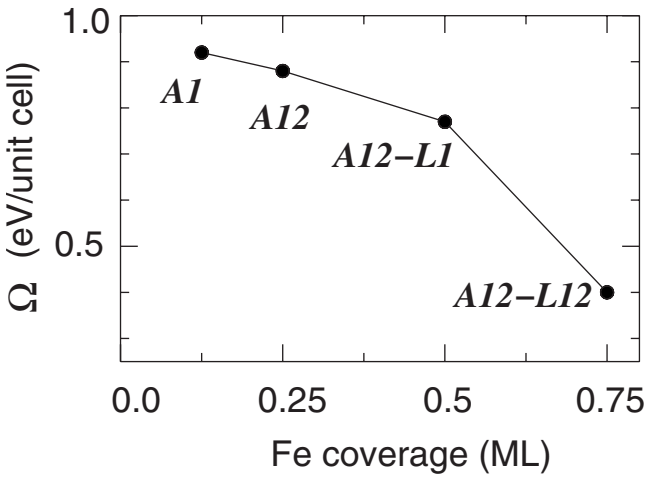

FIG. 2. Formation energy (Ω) of Fe adatoms beside the Bi NLs in their equilibrium geometries, as a function of the Fe coverage per monolayer.

tion energy of this structure is 0.12 eV/unit cell lower than A12-L1, resulting in the most favorable structure under study. Figure 2 shows the formation energy of the most stable configurations as a function of the Fe concentration. These results suggest that controlling the Fe concentration, it would be possible to build up Fe stripes constrained by Bi NLs on hydrogenated silicon surfaces. Similarly to the structural model A12, the A12-L1 and A12-L12 structures show

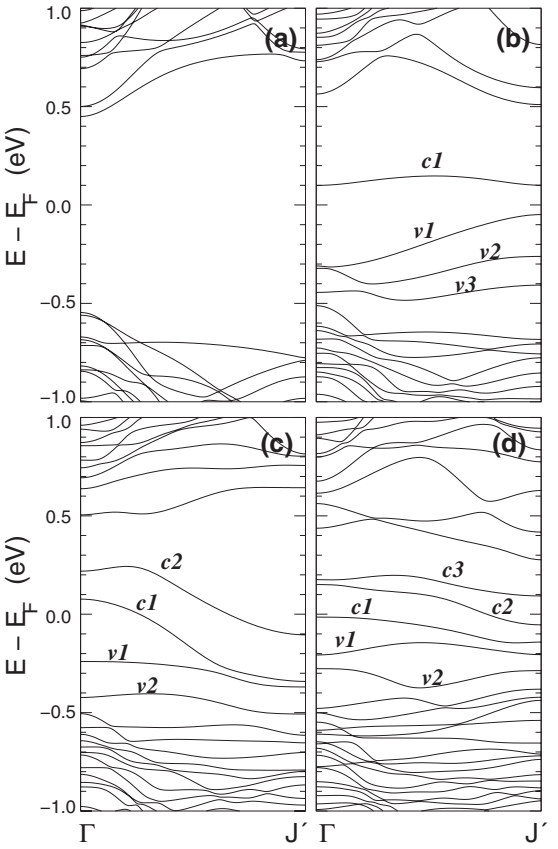

FIG. 3. Electronic band structure of clean Bi lines (a), and structural models A12 (b), A12-L1 (c), and A12-L2 (d). The zero energy is taken as the Fermi level (E_F).

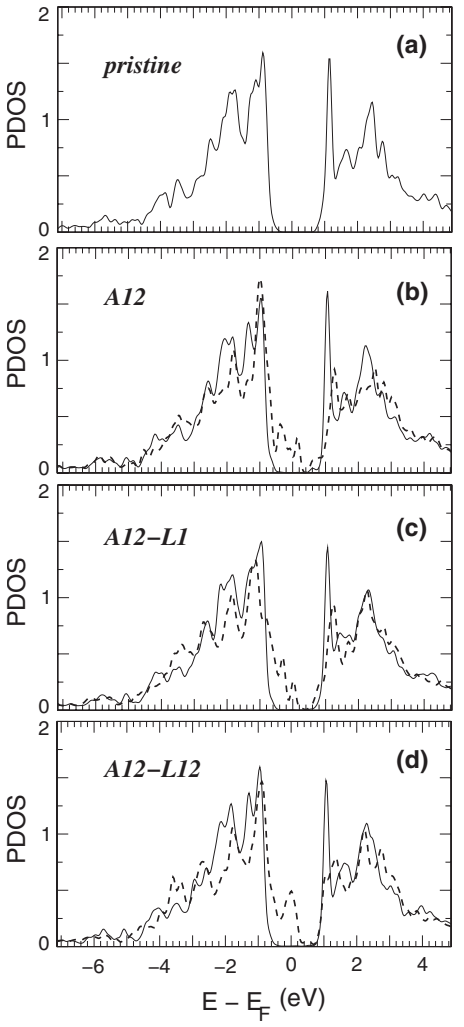

FIG. 4. Projected density of states of the Bi 6*p* orbitals for the pristine Bi line (a), and Fe adsorbed structural models A12 (b), A12-L1 (c), and A12-L12 (d). In (b)–(d), dashed lines (solid lines) represent the density of states of Bi atoms beside (far from) the Fe adsorption sites. The zero energy is taken as the Fermi level (E_F).

AFM and NM states energetically degenerates. This behavior shows that the magnetic state of the Fe adatom in the site A1 is quenched when others Fe atoms approach. It is worth to point out that to get a complete picture of the formation Fe stripes patterned by Bi NLs, the energy barrier for Fe diffusion into silicon bulk is an important issue. However, this is beyond the scope of the present paper.

B. Band structures calculations

Figure 3(a) presents the electronic band structure of the pristine Bi-NL/H/Si(001) surface along $\Gamma J'$, corresponding to the wave vectors parallel to the nanolines. This system exhibits a semiconducting character, where the surface states of the Si dangling bonds are suppressed due to the hydrogen passivation. The occupied (empty) states of Bi dimers are resonant with Si valence (conduction) bands.[12] This is clarified from the projected density of states (PDOS) of the Bi 6*p* orbitals, depicted in Fig. 4(a), which shows that the electronic contribution from the Bi dimers are concentrated at

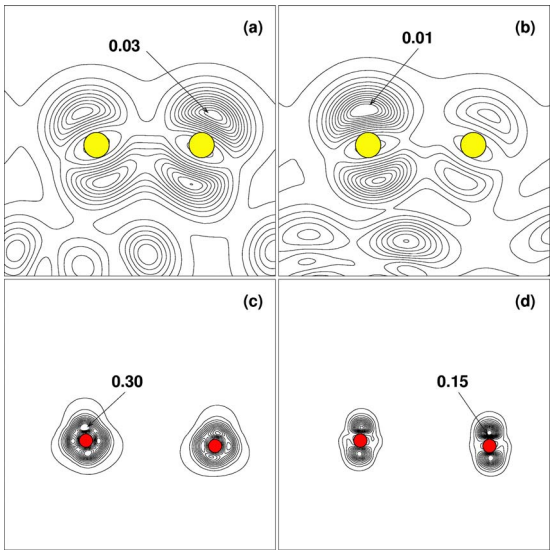

FIG. 5. (Color online) Electronic charge density, within an energy range of 0.5 eV with respect to the Fermi level, for the structural model A12: (a) occupied and (b) empty states along the Bi dimers beside the Fe adatoms, (c) occupied and (d) empty states on Fe adatoms. Units in e/Bohr^3. Plots (a) and (b) depict the charge density on a vertical plane passing through a Bi dimer. Plots (c) and (d) depict the charge density on another vertical plane passing through Fe atoms.

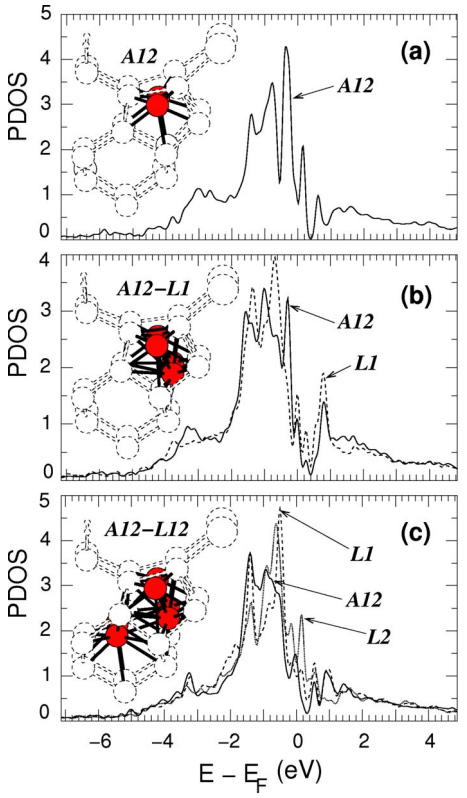

FIG. 6. (Color online) Projected density of states of the Fe 3*d* orbitals for the structural models A12 (a), A12-L1 (b), and A12-L12 (c). The zero of energy is taken as the Fermi level (E_F).

~0.5 eV below (above) the valence (conduction) band maximum (minimum).

The Fe adsorption along the Bi-NLs gives rise to surface states within Si energy band gap. For the structural model A12 the semiconducting character is kept [see Fig. 3(b)]. However, we find four surface states within the energy band gap, $v1-v3$ (occupied) and $c1$ (empty). These electronic states are mainly localized on the Fe adatoms and the nearest-neighbor Bi dimers to the Fe stripe.

Figures 5(a) and 5(c) show the charge density plots associated to the states within $E_F-0.5$ eV and E_F, and within E_F and $E_F+0.5$ eV, respectively. We observe that the occupied states have a contribution from the Bi 6*p* orbitals [Fig. 5(a)] and a stronger contribution from the Fe $3d_{xz}$ orbitals [Fig. 5(c)]. Similar results are found for the unoccupied states [Fig. 5(b)] and [Fig. 5(d)], but here the stronger Fe contribution comes from the $3d_{z^2}$ orbitals. However, in Fig. 5(b) it is noticeable that, different from the occupied states, the unoccupied states are asymmetrically distributed along the Bi dimer. Such asymmetric electronic distribution is attributed to the relaxations of the Bi atoms aside the Fe stripe; for instance, the vertical buckling and the stretch of the Si-Bi bonds observed in the structural model A12.

Figure 4(b) shows that the electronic states of the Bi dimer beside the Fe adsorption sites are perturbed due to the presence of Fe adatoms. In this diagram the dashed line represents the 6*p* orbitals of the nearest-neighbor Bi dimer to the Fe adsorption sites. These orbitals contribute to the formation of the surface states within the energy band gap, while the 6*p* electronic states of the other Bi dimer, far from the Fe adsorption site [solid line in Fig. 4(b)], does not contribute to the $v1-v3$ and $c1$ states. In addition to the 6*p* orbitals from the Bi dimer beside the Fe stripes, as depicted in Fig. 6(a), the (localized) 3*d* orbitals of Fe adatoms also contribute to the formation of surface states within the energy band gap.

The electronic band structures of the A12-L1 and A12-L12 structures, Fig. 3(c) and 3(d), respectively, indicate that the Fe stripes become progressively metallic with the increase in the Fe coverage along the Bi NLs. For the Fe coverage of 1/2 ML we find two partially occupied states, $c1$ and $c2$, with energy dispersion of ~0.2 eV along the $\Gamma J'$ direction. Based upon our PDOS calculations, we verify that the electronic states within the energy band gap come from: (i) Bi dimers beside the Fe adsorption sites [Fig. 4(c)], and (ii) Fe adatoms of the zigzag iron stripes [Fig. 6(b)]. In addition, it is interesting to note that the electronic density of states within the energy band gap increases as a function of the Fe coverage. For a coverage of 3/4 ML, A12-L12, the density of states within the band gap is higher compared with A12 and A12-L1. The PDOS calculations for A12-L12 indicate that the most of the electronic states within the band gap are localized on the 3*d* orbitals of the Fe stripes [Fig. 6(c)], with a contribution from the Bi dimers beside the Fe adatoms [Fig. 4(d)]. In the latter the energy dispersion of Bi 6*p* orbitals increases, indicating that the electronic states of Bi dimers are less localized along the Bi NLs. On the other hand, in Fig. 6(c) the electronic contribution from the 3*d* orbitals of Fe adatoms in second subsurface layer, L2, is higher compared with the electronic contribution of the 3*d* orbitals of Fe adatoms in subsurface interstitial sites A12 and L1.

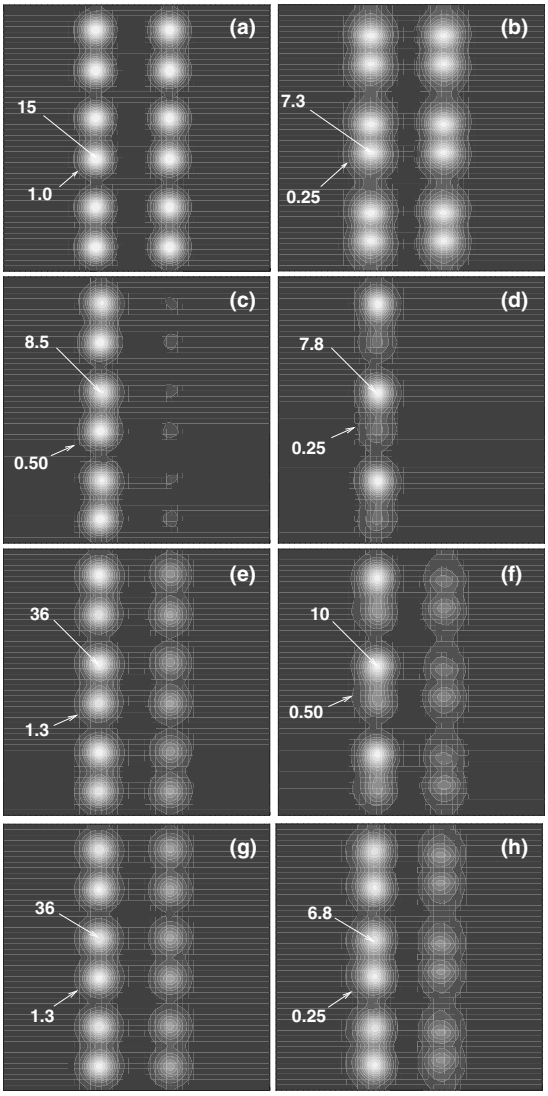

FIG. 7. Electronic density of states projected onto a (001) plane, at 2.5 Å above the topmost Bi dimers, of the pristine Bi-line surface: (a) occupied, and (b) empty states within an energy interval of 1 eV with respect to the Fermi level. For the structural model A12: (c) occupied, and (d) empty states within an energy interval of 0.5 eV with respect to the Fermi level; (e) occupied, and (f) empty states within an energy interval of 1 eV with respect to the Fermi level. For the structural model A12-L12: (g) occupied, and (h) empty states within an energy interval of 1 eV with respect to the Fermi level. Units in 10^{-5} e/Bohr^3.

C. STM calculations

Using the Tersoff-Hamann approximation,[37] we simulate the STM images of Fe stripes patterned by Bi NLs. The electronic states were projected onto a (001) plane at 2.5 Å above the topmost Bi dimers. For pristine Bi NLs, in accordance with previous studies,[12] we find two bright lines along the Bi dimers for the STM images of occupied [Fig. 7(a)] and empty [Fig. 7(b)] states within an interval of 1.0 eV below and above the Fermi level, respectively. These STM images are due to the tunneling current from (to) the occupied π (empty π^*) orbitals lying on the Bi dimers. Figures 7(c) and 7(d) present the STM images of A12 for occupied and empty states, respectively, within energy intervals of $E_F \pm 0.5$ eV. The bright spots are localized on the Bi dimers beside the Fe stripes, where the most of tunneling current comes from the electronic states indicated by dashed lines in Fig. 4(b). It is noticeable that the electronic distribution of the Bi dimers becomes asymmetric due to the formation of Fe stripes, where the Bi dimers far from the Fe adatoms do not contribute to the electronic states within the energy band gap. Indeed, as indicated in Fig. 4 (solid lines), the electronic states of the Bi dimers far from the Fe stripes are weakly perturbed by the presence of Fe adatoms. Such asymmetric distribution of the electronic states on the Bi dimers will change the STM pictures of Fe adsorbed Bi-NL/H/Si(001) surfaces. Even increasing the energy range to $E_F \pm 1.0$ eV, Figs. 7(e) and 7(f), the asymmetric character of STM images is kept, being in consonance with the PDOS calculation, Fig. 4(b). Further examination of our calculated STM images for the empty states, Fig. 7(d) and 7(f), indicates that the brightness of the individual Bi atoms in the dimers is also asymmetric. Namely, one Bi atom is brighter than the other within the same Bi dimer. This result reflects the local relaxation of the Bi dimer for the structural model A12, and the electronic distribution of the unoccupied states along the Bi dimers depicted in Fig. 5(b). In Figs. 7(g) and 7(h) we present the simulated STM images of A12-L12, for the occupied and empty states, respectively, within an energy range of $E_F \pm 1.0$ eV. In these calculated STM images the formation of asymmetric character is mainly due to the electronic distribution along the Bi NLs, as indicated in the PDOS diagram of A12-L12 depicted in Fig. 4(d), since the vertical position of the Bi dimers aside the Fe stripe is 0.04 Å higher compared with the vertical position of the Bi dimers far from the Fe adsorption sites. On the other hand, for the equilibrium geometry, the vertical buckling of the dimer is suppressed in A12-L12, giving rise to symmetric bright spots in the STM images on the individual Bi atoms within the same Bi dimer.

IV. SUMMARY AND CONCLUSION

The formation of iron silicide structures close to the Bi NLs on the H/Si(001) surface has been investigated by *ab initio* total-energy calculations. Our results indicate the formation of energetically stable iron silicide wires parallel to the Bi NLs. These Fe structures are formed in subsurface interstitial sites beside the Bi NLs, showing lower formation energies for increasing Fe concentrations. The electronic properties of these stripes have been examined as a function of the iron coverage. We find that, (i) for low coverage of 1/4 ML (structural model A12), the stripes are semiconducting, and (ii) for iron coverage of 1/2 and 3/4 ML, structural models A12-L1 and A12-L12, respectively, the stripes are metallic. Further electronic structure investigations reveal that the electronic states of Bi NLs become asymmetric due to the presence of Fe adatoms. The electronic states attributed to the $6p$ orbitals of the nearest-neighbor Bi dimers to the Fe adsorption sites contribute to the formation of surface states

within the band gap. In contrast, the electronic states of Bi dimers far from the Fe adatoms are weakly perturbed by the formation of iron stripes. These surface states give rise to asymmetric STM images along the Bi NLs. In addition, for Fe coverages higher than 1/4 ML, the systems exhibit weak antiferromagnetic states which are almost energetically degenerated with their respective nonmagnetic states, suggesting that Fe adatoms have their magnetism quenched as the Fe wire forms.

ACKNOWLEDGMENTS

R. H. Miwa acknowledges financial support from the Brazilian agencies CNPq and FAPEMIG, and the computational support from CENAPAD/SP. W. Orellana acknowledges financial support from the Chilean agencies FONDECYT under Grant No. 1050197 and Anillo Bicentenario through Project No. ACT24/2006. Some of the computational work was carried out at Exeter.

[1] Y. Huang, X. Duan, Q. Wei, and C. M. Lieber, Science **291**, 630 (2001).
[2] P. Mohan, J. Motohisa, and T. Fukui, Appl. Phys. Lett. **88**, 13110 (2006).
[3] P. M. Albrecht and J. W. Lyding, Appl. Phys. Lett. **83**, 5029 (2003).
[4] W. Orellana, R. H. Miwa, and A. Fazzio, Phys. Rev. Lett. **91**, 166802 (2003).
[5] W. Orellana, R. H. Miwa, and A. Fazzio, Surf. Sci. **566-568**, 728 (2004).
[6] R. H. Miwa, W. Orellana, and A. Fazzio, Appl. Phys. Lett. **86**, 213111 (2005).
[7] P. M. Albrecht and J. W. Lyding, Small **3**, 146 (2007).
[8] R. H. Miwa and G. P. Srivastava, Surf. Sci. **473**, 123 (2001).
[9] T. Uchihashi, C. Ohbuchi, S. Tsukamoto, and T. Nakayama, Phys. Rev. Lett. **96**, 136104 (2006).
[10] T. Abukawa, M. Sasaki, F. Hisamatsu, T. Goto, K. Kinoshita, A. Kakizaki, and S. Kono, Surf. Sci. **325**, 33 (1995).
[11] H. W. Yeom *et al.*, Phys. Rev. Lett. **82**, 4898 (1999).
[12] R. H. Miwa, J. M. MacLeod, A. B. McLean, and G. P. Srivastava, Nanotechnology **16**, 2427 (2005).
[13] J. M. MacLeod and A. B. McLean, Phys. Rev. B **70**, 041306(R) (2004).
[14] M. Naitoh, H. Shimaya, S. Nishigaki, N. Oishi, and F. Shoji, Surf. Sci. **377-379**, 899 (1997).
[15] K. Miki, J. H. G. Owen, D. R. Bowler, G. A. D. Briggs, and M. Sakamoto, Surf. Sci. **421**, 397 (1999).
[16] R. Miwa and G. Srivastava, Surf. Sci. **600**, 4048 (2006).
[17] J. Owen and K. Miki, Nanotechnology **17**, 430 (2006).
[18] J. Owen and K. Miki, Surf. Sci. **600**, 2943 (2006).
[19] H. Koga and T. Ohno, Phys. Rev. B **74**, 125405 (2006).
[20] M. Fanciulli, G. Weyer, A. Svane, N. E. Christensen, H. von Känel, E. Müller, N. Onda, L. Miglio, F. Tavazza, and M. Celino, Phys. Rev. B **59**, 3675 (1999).
[21] S. Walter, R. Bandorf, W. Weiss, K. Heinz, U. Starke, M. Strass, M. Bockstedte, and O. Pankratov, Phys. Rev. B **67**, 085413 (2003).
[22] K. Kataoka, K. Hattori, Y. Miyatake, and H. Daimon, Phys. Rev. B **74**, 155406 (2006).
[23] G. Profeta, S. Picozzi, A. Continenza, and R. Podloucky, Phys. Rev. B **70**, 235338 (2004).
[24] H. Wu, P. Kratzer, and M. Scheffler, Phys. Rev. B **72**, 144425 (2005).
[25] D. P. Adams, L. L. Tedder, T. M. Mayer, B. S. Swartzentruber, and E. Chason, Phys. Rev. Lett. **74**, 5088 (1995).
[26] T. Kishi, K. Suzuki, D. Matsuoka, W. A. Diño, H. Nakanishi, and H. Kasai, J. Phys.: Condens. Matter **16**, S5763 (2004).
[27] A. Kida, H. Kajiyama, S. Heike, T. Hashizume, and K. Koike, Appl. Phys. Lett. **75**, 540 (1999).
[28] P. Hohenberg and W. Kohn, Phys. Rev. **136**, B864 (1964).
[29] J. P. Perdew and A. Zunger, Phys. Rev. B **23**, 5048 (1981).
[30] X. Gonze, R. Stumpf, and M. Scheffler, Phys. Rev. B **44**, 8503 (1991).
[31] D. Vanderbilt, Phys. Rev. B **41**, 7892 (1990).
[32] S. Baroni, A. Dal Corso, S. de Gironcoli, P. Giannozzi, C. Cavazzoni, G. Ballabio, S. Scandolo, G. Chiarotti, P. Focher, A. Pasquarello, K. Laasonen, A. Trave, R. Car, N. Marzari, and A. Kokalj (http://www/pwscf.org).
[33] R. H. Miwa and G. P. Srivastava, Phys. Rev. B **66**, 235317 (2002).
[34] R. H. Miwa, J. M. MacLeod, A. B. McLean, and G. P. Srivastava, Nanotechnology **17**, 1803 (2006).
[35] J. H. G. Owen, K. Miki, H. Koh, H. W. Yeom, and D. R. Bowler, Phys. Rev. Lett. **88**, 226104 (2002).
[36] W. Orellana and R. Miwa, Appl. Phys. Lett. **89**, 93105 (2006).
[37] J. Tersoff and D. R. Hamann, Phys. Rev. B **31**, 805 (1985).